Proc. Natl. Acad. Sci. USA
Vol. 85, pp. 4971–4975, July 1988
Biochemistry

Comparison of time-resolved and -unresolved measurements of deoxyhemoglobin in brain

B. CHANCE*†, J. S. LEIGH*, H. MIYAKE*, D. S. SMITH‡, S. NIOKA*, R. GREENFELD*, M. FINANDER§, K. KAUFMANN¶, W. LEVY‡, M. YOUNG‡, P. COHEN‡, H. YOSHIOKA*, AND R. BORETSKY*

Departments of *Biochemistry/Biophysics and ‡Anesthesia, University of Pennsylvania, Philadelphia, PA 19104; †Institute for Structural and Functional Sciences, 3401 Market Street, Room 320, Philadelphia, PA 19104; §Coherent Laser Products Division, P.O. Box 10321, Palo Alto, CA 94303-9965; and ¶Hamamatsu Photonics Systems Corp., 360 Foothill Road, P.O. Box 6910, Bridgewater, NJ 08807-0910

Contributed by B. Chance, February 23, 1988

ABSTRACT **Continuous (CW) and pulsed light were used for the noninvasive measurement of hemoglobin oxygenation in tissues. A dual wavelength method of continuous illumination spectroscopy used 760 nm (deoxyhemoglobin peak) and 800 nm (an oxyhemoglobin–deoxyhemoglobin isosbestic point) to measure the kinetics and extent of oxyhemoglobin deoxygenation in brains during mild ischemia/hypoxia. Absorption and scattering were modeled in an artificial milk/yeast blood system, which gave an exponential relationship between absorption and optical path length to a depth of 7 cm. Time-resolved spectroscopy (10-ps resolution) afforded a display of the times and distances of arrival of photons emitted by the cat brain in response to a 10-ps input pulse. The emitted photons rose to a peak in a fraction of a nanosecond and declined exponentially over a few nanoseconds. The half-time of exponential decay corresponds to photon migration over a distance of 4 cm. Exponential light emission continued for several more nanoseconds when the brain was encased by the skull, which plays a key role in prolonging light emission. The exponential decline of light intensity has a value [exp($-\mu L$)], where L is the path length determined from the time/distance scale and μ is the characteristic of the migration of light in the brain. The factor μ is increased by increasing absorption, and $\mu' = \varepsilon C$ where ε and C are the Beer–Lambert parameters of extinction coefficient (ε) and concentration (C). Thus, deoxyhemoglobin can be quantified in brain tissues.**

The utility of optical methods in studying metabolism and oxidative processes in cells and tissues was significantly enhanced in the early 1950s when a time-sharing dual-wavelength system was developed for the quantitation of small changes in absorption in a highly scattering medium such as cell suspensions or muscle tissues in the visible and near-infrared (NIR) regions (1, 2). Fluorescence signals from mitochondrial NADH complemented the absorption method for studies of the surface of heart, brain, and skeletal tissue (3, 4). NIR spectroscopy was used to detect the redox state of the copper component of cytochrome oxidase in mitochondria (2) and yeast cells (5), and Jobsis-VanderVliet and coworkers (6–8) pioneered the study of NIR absorption in tissues by transillumination. More recently, algorithms have been developed by vanderZee and Delpy (9) to compensate for the interference from hemoglobin and myoglobin with cytochrome copper, as the latter may constitute as little as 10% of the total signal at 830 nm (see also ref. 10).

This paper compares the use of continuous (CW) and pulsed light. The CW method has been applied to both animal and model systems to determine: (*i*) the attenuation characteristic of the light in models containing localized deoxyhemoglobin (Hb) and (*ii*) the ability to observe hypoxia in the brains of human subjects.‖ However, CW systems fail to quantify concentrations because they do not measure the optical path.

The pulsed-light system time-resolves the emergence of light pulses from the brain; picosecond NIR lasers and a streak camera are used to time-resolve the photons scattered by the brain tissue and thus obtain the path length (L) of the emergent light.

THEORETICAL

After an instantaneous input light pulse, the detected "output" light intensity rises to a maximum and then decays. In the presence of light-absorbing material, the decaying portion of the detected output is dominated at relatively long times by an exponential form:

$$I(t) \simeq I_o \exp(-2.303\ kt). \quad [1]$$

This equation is simply a consequence of the Beer–Lambert law:

$$I(t) = I_o \exp(-2.303\ \varepsilon[C]L) \quad [2]$$

with ε the classical extinction coefficient, $[C]$ the concentration of absorber, and L the path length. The appropriate path length is simply related to t, the "time of flight," by:

$$L = ct/n \quad [3]$$

with, c, the velocity of light and n the average refractive index; for water, $n = 1.33$ and $c \simeq 23$ cm/ns.

Thus, from a semilogarithmic plot of the detected light intensity, we obtain an approximately straight line with a negative slope, $\mu = \varepsilon[C]\ c/n$. For observation of changes in absorption (say, by deoxygenation of HbO_2), then the concentration of absorber may be calculated from the change in slope μ:

$$[C] = \frac{n}{c}\frac{\Delta\mu}{\Delta\varepsilon}. \quad [4]$$

From Eq. 2, we obtain

$$\log\frac{I_o}{I} = \varepsilon[C]L \quad [5]$$

The publication costs of this article were defrayed in part by page charge payment. This article must therefore be hereby marked "*advertisement*" in accordance with 18 U.S.C. §1734 solely to indicate this fact.

Abbreviations: NIR, near infrared; EEG, electroencephalogram; FiO_2, fraction inspired oxygen; HbO_2, oxyhemoglobin; Hb, deoxyhemoglobin total (or unspecified state) hemoglobin.

‖These studies were approved by the Committee on Studies Involving Humans, University of Pennsylvania. Informed consent was obtained from each subject.

and plot log I_o/I versus L (as illustrated in Fig. 5).

$$\frac{1}{L}\log\frac{I_o}{I} = \mu = \varepsilon[C]. \quad [6]$$

Units are: L, cm; ε, $cm^{-1}\cdot mM^{-1}$; C, mM; and μ, cm^{-1}.

We may compare CW and pulsed-light (PL) results,

$$\mu_{CW} = \varepsilon\Delta C = \frac{1}{L_{CW}}\left(\log\frac{I_o}{I}\right)_{CW}, \quad [7]$$

because equal $\varepsilon\Delta C$ changes are readily obtained for both methods and give $\Delta\mu_{PL}$ for pulsed light and log $(I_o/\Delta I)_{CW}$ for the CW method:

$$L_{CW} = \frac{(\log I_o/\Delta I)_{CW}}{\Delta\mu_{PL}}. \quad [8]$$

Thus, the path length of the CW system can be calibrated by the PL system.

$L_{1/2}$ is defined as the length (abscissa of Fig. 5) for a decrease of I from its maximum I_o to $I/2$.

$$L_{1/2} = \frac{0.301}{\mu} \quad [9]$$

For a change of ε or C,

$$L_{1/2} = \frac{0.693}{\Delta\varepsilon\Delta C}. \quad [10]$$

The experimental results of Table 1 are given as μ (cm^{-1}) and $L_{1/2}$ in columns 6 and 7. $L_{1/2}$ is a "characteristic length" that is maximum when the hemoglobin concentration is zero as in the cat-head model or when the wavelength is chosen for minimal Hb absorption. For the cat brain, $L_{1/2}$ = 6.7 cm, and for the human brain, $L_{1/2}$ = 4.3 cm.

METHODS

CW. Excitation at 760 and 800 nm is time-shared through a single fiber-optic light guide. The detectors (Hamamatsu R928) have a high signal-to-noise ratio because of their measurement of light emitted from a large area (2 cm^2 per detector). Light input and output are separated by 2 cm. A barrier minimizes specular and short path reflections.

Hemoglobin Absorption. The important spectral parameters of HbO_2 and Hb required are the differences between their extinction coefficients at 760, 790, and 800 nm. These are 0.25, 0.086, and <0.01 $cm^{-1}\cdot mM^{-1}$, respectively. At a typical brain Hb value of 0.15 mM, a $\Delta\mu$ of 0.038 cm^{-1} at 760 nm would be expected in the cat brain on deoxygenation with normal hematocrit and no light scattering.

Milk Model. To simulate the presence of the skull and to quantify the detection of HbO_2 deoxygenation within a light-scattering volume (9, 10), we have used the model of Fig. 1. The larger vessel (5.5-cm diameter) is filled with a tissue substitute (artificial milk derivative) adjusted to mimic the NIR light-scattering property of the skull. Inside this container is a second vessel containing 100–200 μM Hb and bakers' yeast with an equivalent scattering power to simulate the blood-perfused brain tissue. The yeast respiration causes a continuous deoxygenation of HbO_2 so that determination of its absorption changes simulates anoxia in the brain. The internal vessel is moveable with respect to the external one so that a scattering volume of variable depth is interposed between the two.

Time-Resolved Spectroscopic Method. To calculate penetration depths in brain, we studied the time resolution of the photon migration within various tissues and the models. The absorption of visible and NIR light in highly scattering material has been described by Duysens (11) and Chance (3, 12) and more recently by Blumberg (13), vanderZee and Delpy (9), and Bonner *et al.* (14). The light is multiply scattered so that directionality is lost after a few scattering lengths (13). Thus, the duration of a short pulse of radiation introduced into a highly scattering object, such as the brain, will be observed to be greatly prolonged because of photon migration to the receiver site. When there is a specific absorber such as Hb (measured at 760 nm), the number of photons detected will be appropriately diminished.

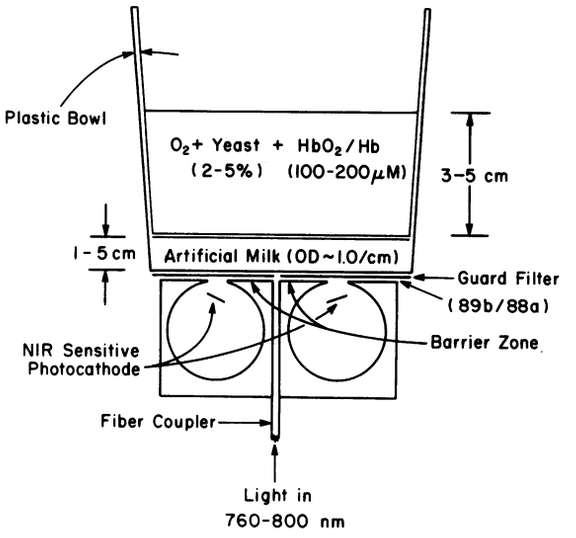

FIG. 1. The model NIR spectrometer system for testing the penetration of light in brain.

Optical System. Two synchronously pumped, tunable dye lasers (Coherent Laser Products Division), operating at 760 and 790 nm and pumped by the second harmonic of a CW NdYAG (neodymium/yttrium/aluminum-garnet) mode-locked laser, were used as the light source. The pulse length was 6 ps, the pulse energy was 1.3 nJ per pulse, and the average power was 100 mW at 77 MHz. The decay of the radiation was recorded with a 0.2-cm fiber-optic probe coupled to a streak camera (Hamamatsu). The fibers were placed at various positions with respect to the input light to record the migration of light to the exit fiber. The velocity of light, c/n, in the brain tissue is taken to be 0.023 cm/ps for a refractive index of 1.3. The signal-to-noise ratio was adequate for 3 decades of logarithmic plot. The time-difference determinations are accurate to 10 ps.

Preparation of the Cat Head and Brain. To evaluate the changes in photon migration that occur when a known concentration (0.15 mM) of Hb is added to a localized region of brain, the cat-head model met the following requirements: (*i*) the brain was initially hemoglobin free, (*ii*) there was a portion of brain into which Hb could be injected and in which Hb would be stable, (*iii*) the brain could be observed without or with the skull (termed cat head), and (*iv*) it could be transported readily. This model involves redistribution of K^+, Na^+, and H_2O that occur on death. However, the values of μ do not differ greatly from the *in vivo* condition, 0.08 as compared to 0.07 cm^{-1} (B.C., unpublished data).

The animal was anesthetized with ketamine and heparinized (400 units/kg of body weight). The head was cleared of blood by exchange transfusion with Ringer's solution, which was followed by 10% (vol/vol) glycerol. Experimental observations were made before and after perfusion of one hemisphere (via the cannulated carotid artery) with Hb in blood cells at a normal hematocrit (40%). Subsequent analysis of the distribution of the hemoglobin showed 35 μM and 63 μM in the two hemispheres after reperfusion with blood.

The geometry of the cat-head model is illustrated in Fig. 2, which indicates the point of input of the laser light and the points at which a 0.2-cm diameter fiber probe was attached to obtain output signals. The points were chosen to corre-

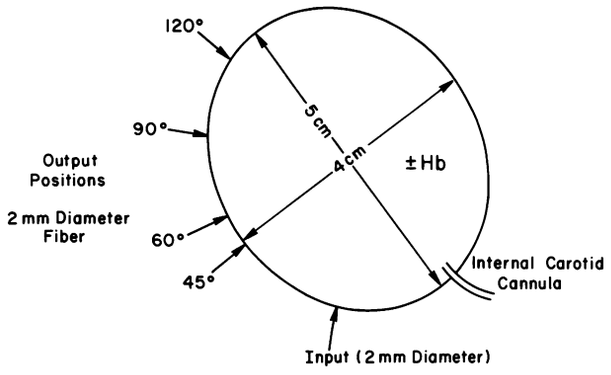

FIG. 2. Pulsed-light study: diagram of the cat-head model, indicating the location of the input and output fibers together with location of the middle cerebral artery by which Hb was injected into the contralateral hemisphere.

spond to the 2.0-cm separation of the milk model and three additional 3.0-, 5.0-, and 6.5-cm points at angles of 45°, 60°, and 90° and 110°, respectively.

RESULTS

Milk Model System. Since the effect of distance between the light input and the hemoglobin-containing compartment can be varied in the model system (Fig. 1), a plot of the signal caused by deoxygenation of 200 μM HbO_2 can be displayed as a function of optical path through the milk substitute. The Hb/HbO_2 signal decreased logarithmically as the length of the optical path through the milk substitute-containing vessel was increased from 2 to 7 cm (Fig. 3). The slope was 0.014 cm^{-1}, and the ΔOD extrapolated to zero thickness of the milk layer was 0.06. This may be compared with a $\Delta\mu$ value of 0.050 cm^{-1} as calculated from the increment of the extinction coefficient (0.25 $cm^{-1} \cdot mM^{-1}$) with 760 nm as a measuring wavelength and 800 nm as a reference wavelength (see Table 1).

Adult Human Brain Studies. The spectrophotometer was applied to the temporal region of the head of two volunteer human subjects. Breathing graded decreases of oxygen caused the HbO_2 to become partially deoxygenated (Fig. 4). Each subject's electroencephalogram (EEG) was also monitored and showed corresponding changes as oxygen delivery decreased. The EEG began to show altered activity as the inspired oxygen (FiO_2) decreased to 0.10. The changes become marked at an FiO_2 of 0.065, and this corresponded to the lowest degree of hemoglobin saturation. Immediately upon the subject's breathing room air, all parameters returned rapidly to normal. The total ΔOD was 0.18. The concentration change

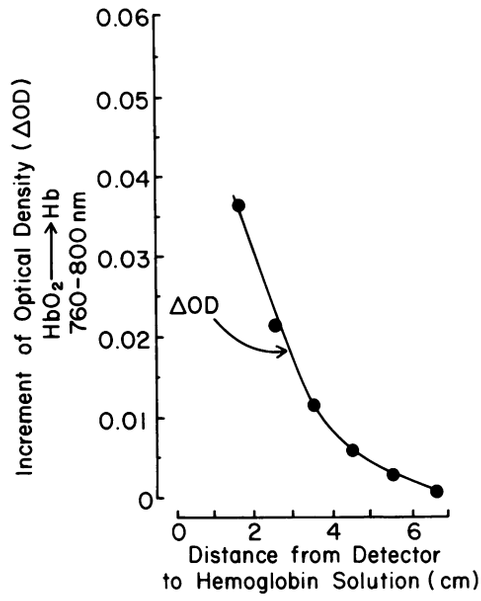

FIG. 3. Illustration of the effect of path length, L, upon the HbO_2–Hb signal in the upper chamber of Fig. 1. The absorbance decreases logarithmically with L.

cannot be calculated without an estimate of the effective path length, L. For the expected value for 150 μM Hb, the apparent optical path is 5.0 cm (see *Discussion*). Similar results were obtained with both individuals.

Time-Resolved Spectroscopy. *Decay kinetics.* The decay kinetics are accurately exponential over 2–3 logarithmic decades, corresponding to $\approx$1 ns or a distance of >20 cm. In the milk model, an angle of 135° or a 6.5-cm path was required to obtain a 2-decade single exponential fit to 100-ps accuracy. In the cat head (and dog head; B.C., unpublished data) and human heads (B.C., unpublished data) curvature in the logarithmic slope of the homogeneously perfused head was observed when a bony structure intervened—i.e., the frontal sinuses in the adult human.

Table 1 gives a number of properties of the light-pulse output of several models to a picosecond-light-pulse input. The outputs are evaluated by several criteria: the pulse width; the angle between light input and output (Table 1, column 3; and Fig. 2); the logarithmic slope, μ; and $L_{1/2}$. The short pulse observed in reflection from a surface in water (40 ps) was broadened to 110 ps in the milk model, to nearly 500 ps in the preserved cat brain and in the adult human brain (B.C., unpublished data). The criterion of interest here is the slope of the experimental decay (Table 1, column 6).

Table 1. Properties of models

Sample (Fig.)	λ, nm	Angle, °	Distance, mm	Half-width, ps	μ, cm^{-1}	$L_{1/2}$, cm
Water	760	—	—	40		
Milk substitute	760	110	65	110	0.088	3.4
+ HbO_2	760	110	65	150	0.083	3.6
+ Hb	760	110	65	108	0.105	2.8
+ Hb	790	110	65	105	0.088	3.4
+ HbO_2	790	110	65	142	0.081	3.7
Cat head (5)	760	90	42	450	0.068	4.5
+ Hb (5)	760	90	42	350	0.081	3.4
+ Hb (5)	790	90	42	430	0.072	4.2
+ Hb (5)	760	90	42	350	0.084	3.6
	790	90	42	470	0.054	5.6
Cat brain	760	60	24	300	0.114	3.6
	790	60	24	300	0.117	3.6
	790	90	42	290	0.090	3.3

Effect of hemoglobin. Fig. 5 *A* and *B* shows data obtained from the cat head before and after Hb injection at an angle of 90°, which corresponds to a 4.2-cm distance between light input and output. In the absence of Hb, the half-width or scattering-time constant was 450 ps. When Hb was added to the contralateral hemisphere, a value of 360 ps was obtained. The values of μ were 0.068 cm^{-1} and 0.081 cm^{-1}, and $L_{1/2}$ values were 6.7 and 4.8 cm, respectively.

Effect of wavelength. In Fig. 5 *C* and *D*, the effect of wavelength upon the decay kinetics was measured at 760 and 790 nm. The angle between incidence and recording was 90°. The specificity of wavelength dependence is shown; the waveform decays more rapidly with 760-nm light than with 790-nm light. The scattering time constant at 790 nm is 430 ps, which decreases to 350 ps at 760 nm. The μ values are 0.072 and 0.084 cm^{-1}, and the $L_{1/2}$ values are 5.8 and 4.2 cm, respectively.

Effect of separation of input and output. The optical path length is not well defined in CW illumination (9, 13), and we wished to determine the effective path lengths actually used in the CW study of Fig. 4. In Table 1 we have summarized the values of μ for a variety of angular positions and distances on the circumference on the brain, all measured with respect to the input pulse. In the cat brain, 45° and 60° give the same result, and 90° gives a 20% increase of lifetime (a 20% decrease of slope). The corresponding separations are 2.0, 3.0, and 5.0 cm. Thus, the decay rate of light observed does not depend critically upon the location of the fibers. This validates that the 2.0-cm separation of input and output used with the continuous illumination of the human brain, gives a penetration of 50% of the emitted light to several centimeters.

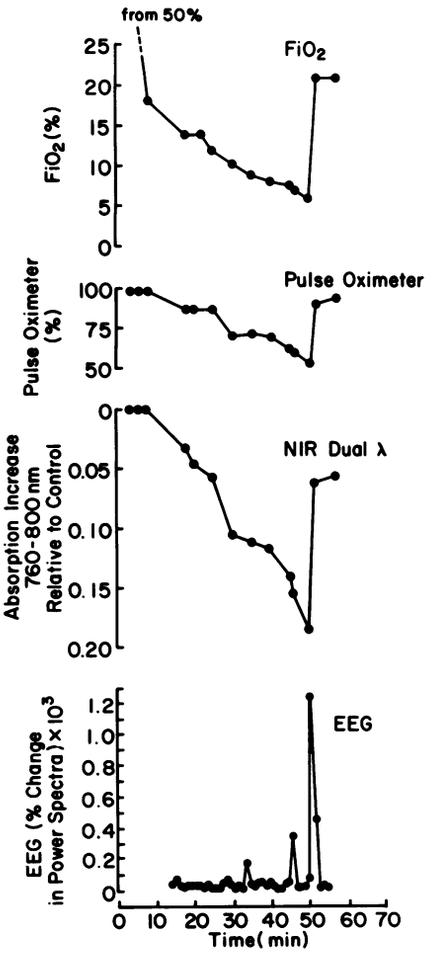

FIG. 4. Systemic hypoxia NIR monitor of adult human brain. Continuous light study: stack plot of FiO_2, pulseoximeter, NIR dual wavelength absorbance, and EEG for a human subject breathing inspired oxygen which changed from 50% to 7% over the course of 40 min. Thereafter room air was breathed. The chart shows the sensitive response of the NIR to increasing hypoxia.

DISCUSSION

Comparison of CW and Pulsed-Light Study. The studies with pulsed-light illumination establish the potential of the two wavelength approach to *in vivo* NIR reflectance spectroscopy. The origin of the signal is calculated to be in the capillary bed as follows: each anoxic erythrocyte absorbs 1% at 760 nm; thus, at a hematocrit of 0.4, light can transit ≈50 capillaries with a 20% absorption. With a typical intercapillary distance of 50 μm, this corresponds to 50% transmission over a distance of ≈3 cm. Larger blood vessels will extinguish the photons in a single pass. Thus a "mixed" arterial venous signal is obtained and, in the animal brain study, correlates with changes of the phosphocreatine/inorganic phosphate (PCr/P_i) ratio and the reduction of cytochrome oxidase aa_3 when the hemoglobin signal indicates 80–90% deoxygenation (10). In this way, the deoxygenation of HbO_2 in the range of up to 80% gives early warning of changes in the phosphocreatine/P_i ratio and cytochrome aa_3 (7).

Fig. 4 shows that the CW measurements correlate with changes in the EEG, which is also a measure of brain oxygen availability during hypoxia. The difference between NIR spectroscopy of the human head and visible spectroscopy of the finger (pulse oximeter) is consistent with the above suggestion that the NIR data represent brain capillary hemoglobin. Deoxygenation in the adult gives a ΔOD of at least 0.18. The high rate of oxygen utilization of the brain affords a high sensitivity of arterial venous oxygen content for the detection of early ischemia.

The NIR CW signals (2-cm^2 area for each detector in the milk model) give an apparent μ of 0.06 cm^{-1} for the detection of hemoglobin signals in the model of Fig. 1. However, the hemoglobin concentration is underestimated by interposing the nonhemoglobin-containing barrier—a loss of ≈25% per cm. The pulsed-light data for the milk model give a μ of 0.083 cm^{-1}. The cat brain gives a μ = 0.081 cm^{-1}, a value similar to that of the milk model. The latter values change only 20% when the spacing of the light input and output is increased from 2.0 to 5.0 cm. The human head gives a μ = 0.07 cm^{-1} and $L_{1/2}$ = 4.0 cm (B.C., unpublished data). These values suggest the applicability of the milk model and the cat-brain model to the CW data of Figs. 3 and 4. Thus, it appears that a simple dual-wavelength CW spectrometer (Fig. 1) can measure the state of hemoglobin oxygenation within the brain.

The Effect of Boundary Conditions. It is recognized that the boundary conditions may have a large effect upon the apparent length of photon diffusion. The effect of reflections from the skull is large and prolongs the half-time from 290 to 470 ps at 90°, producing an increase in the $L_{1/2}$ values from 3.3 to 5.6 cm. Other effects due to the frontal sinuses are readily observed, and fast passage through the subarachnoid space, etc., seems to be observable. In fact, when the spacing of input and output exceeds 10 cm, the $L_{1/2}$ appears to decrease, suggesting that "transcranial" geometries may be suboptimal (6, 7).

Quantitation of Time-Resolved Studies. Eqs. 1–4 indicate how quantitative results can be obtained in scattering tissues. Table 1 shows two types of perturbations of μ, by hemoglobin (Hb and HbO_2) concentrations and the presence or absence of hemoglobin and by change of wavelength. In the center portion of the milk model, the Hb/HbO_2 (0.15 mM Fe) change at 760 nm gives a $\Delta\mu$ of 0.022 cm^{-1}. In the contralateral portion of the brain, the injection of 0.15 mM Hb gave a μ of 0.023 cm^{-1}. That these are specific absorption effects

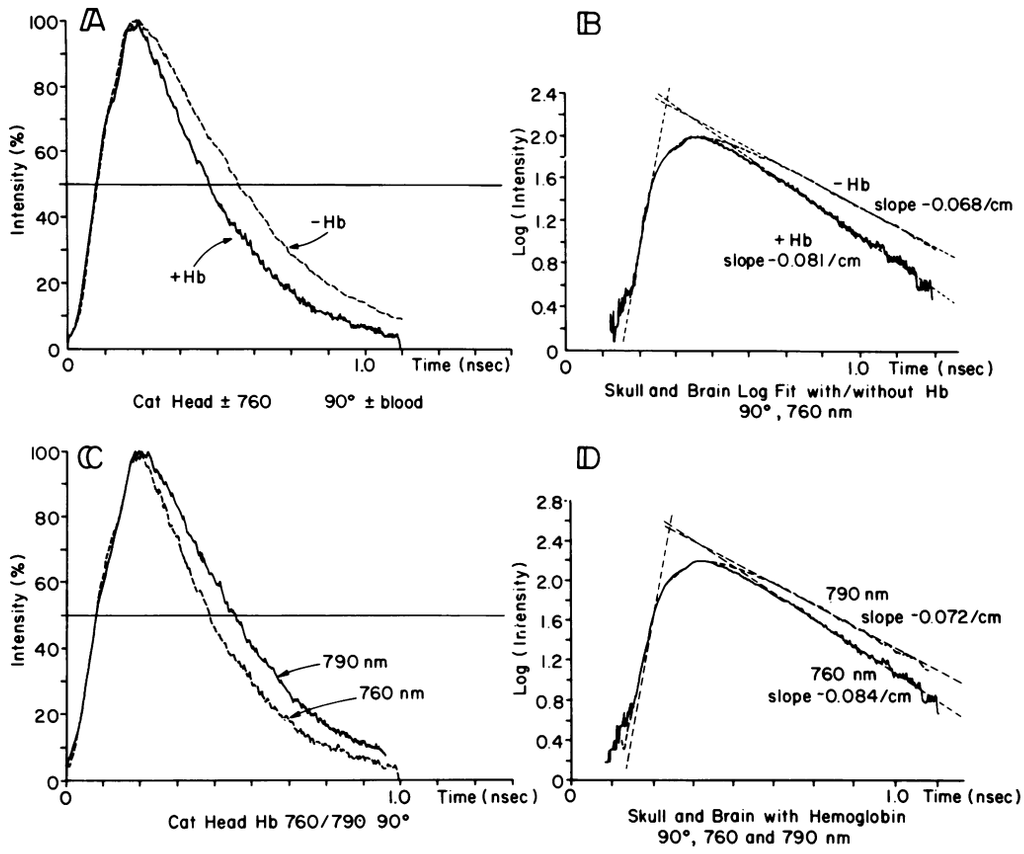

FIG. 5. Pulsed light study: the effect of the presence of hemoglobin in the contralateral hemisphere upon the relaxation of absorption in the cat-head model. (*A*) Linear scale. (*B*) Logarithmic scale. (*C*) Effect of an alteration of wavelength in the cat-head model from 790 nm (near an isosbestic point) to 760 nm, a point at which the Hb absorbs maximally in this region. (*D*) Logarithmic scale.

is supported by the change of wavelength from 760 to 790 nm: $\Delta\mu$ is 0.017 and 0.002 cm^{-1} for 0.15 mM Hb and HbO_2, respectively. In the cat brain, $\Delta\mu$ is 0.011 cm^{-1} corresponding to 44 μM as compared with 35 and 65 μM in the two hemispheres, or 50 μM. Since the goal of these experiments was to ensure the diffusion of light into the center of the milk model and into the contralateral hemisphere of the cat-brain model, we would expect only a fraction of the Hb added to be found. In the milk model, 0.09 mM is found ($\Delta\varepsilon$ = 0.25 $cm^{-1}\cdot mM^{-1}$), and in the cat brain, 0.050 mM is found.

Thus, one would expect at least 150 μM hemoglobin would be found in Fig. 4 and that the path-length estimate of 5.0 cm is a good approximation for the 4-cm^2 aperture hemoglobinometer. The wavelength dependence of the scattering is too small to be detected when the wavelength is changed from 790 to 760 in the cat brain. Thus, the dual-wavelength determination of hemoglobin seems unaffected. It appears that the time-resolved method greatly increases the usefulness of optical spectroscopy in tissue.

Prognostications for the Future. The pulsed-light study affords key information on the penetration obtained with the simpler CW method and validates input/output spacings of 2.0 cm and upwards for the simpler system. The detection of tissue volumes containing Hb is demonstrated by using time-resolved spectroscopy. In large objects, the requirements of a system may be relaxed to permit 20- to 50-ps input light pulses (available from NIR laser diodes in the IR region) to obtain the scattered light decay over 3 decades of intensity. Highly significant information appears to be available in the Beer–Lambert law dependence of the relaxation times, particularly for the detection of *C* and ε. It appears that a deconvolution theorem based upon multiple wavelengths and multiple input/output sites may also shed light on the imaging problem.

The pleasant cooperation of V. Fossati and the staff of Coherent Laser Products Division and of Mr. Teruo Hiruma and the staff of Hamamatsu Photonics are gratefully acknowledged. The support was provided by Otsuka Electronics and by Phospho Energetics. D.S.S. was supported in part by National Research Service Award HL-07286 from the National Institutes of Health. Some of the animal studies were supported in part by National Institutes of Health grant NS 23859.

1. Chance, B. (1951) *Rev. Sci. Instrum.* **22**, 619–627.
2. Chance, B. (1966) in *Biochemistry of Copper*, ed. Peisach, J. (Academic, New York), pp. 293–303.
3. Chance, B., Legallais, V. & Schoener, B. (1962) *Nature (London)* **195**, 1073–1075.
4. Chance, B. (1954) *Science* **120**, 767–775.
5. Chance, B. (1959) *J. Biol. Chem.* **234**, 3036–3040.
6. Jobsis-VanderVliet, F. F. (1985) *Adv. Exp. Med. Biol.* **191**, 833–842.
7. Jobsis, F. F., Keizer, J. H., LaManna, J. C. & Rosenthal, M. (1977) *J. Appl. Physiol.* **113**, 858–872.
8. Rosenthal, M., LaManna, J. C., Jobsis, F. F., Levasseur, J. E., Kontos, H. A. & Patterson, J. L. (1976) *Brain Res.* **108**, 143–154.
9. vanderZee, P. & Delpy, D. T. (1988) in *Oxygen Transport to Tissue X*, eds. Mochizuki, M., Honig, C. R., Koyama, T., Goldstick, T. K. & Bruley, D. F. (Plenum, New York), pp. 191–197.
10. Tamura, M. H., Hazeki, O., Nioka, S., Chance, B. & Smith, D. S. (1987) in *Chemoreceptors and Reflexes in Breathing*, ed. Lahiri, S. (Oxford, New York), in press.
11. Duysens, L. (1964) *Prog. Biophys. Mol. Biol.* **14**, 1–104.
12. Chance, B. (1952) *Nature (London)* **169**, 215–230.
13. Blumberg, W. E. (1987) *Biophys. J.* **51**, 288 (abstr.).
14. Bonner, R. F., Nossal, R., Havlin, S. & Weiss, G. H. (1987) *J. Opt. Soc. Am. Sec. A* **4**, 423–432.